PERGAMON

International Journal of Heat and Mass Transfer 45 (2002) 2755–2768

International Journal of HEAT and MASS TRANSFER

www.elsevier.com/locate/ijhmt

A formal averaging procedure for radiation heat transfer in particulate media

J.L. Consalvi, B. Porterie *, J.C. Loraud

IUSTI CNRS UMR 6595, Technopôle de Château-Gombert, 5 Rue Enrico Fermi, 13453 Marseille cedex 13, France

Received 20 November 2000; received in revised form 25 July 2001

Abstract

Radiative heat transfer in participating particulate media is modeled using a formal volume averaging procedure. The multiphase medium is composed of emitting–absorbing–scattering phases, i.e., a gas phase and several particle phases. Each particle phase contains large, opaque, gray, diffuse, and spherical particles having locally the same geometrical, thermophysical, and radiative properties. The resulting multiphase radiative transfer equation (MRTE) is solved using the discrete ordinates method. The present computed results are found to be in good agreement with those obtained using the Monte-Carlo theory and with the available experimental results. The coupling effect of the MRTE with the averaged energy equations in a three-dimensional cavity which is differentially heated or which contains a volumetric heat source is studied. A parametric study is performed for particle-phase and gas properties, and wall emissivity.

1. Introduction

The basic physical phenomenon of radiation in particulate media is the change in radiative intensity by absorption and/or scattering which occurs during the interaction of an electromagnetic wave or a photon with a medium containing particles. The understanding of this phenomenon has given rise to a large number of works initiated by astrophysicists interested in the scattering of starlight by interstellar dust. The atmospheric science community is also concerned with the scattering of solar radiation, the back-scattering and attenuation of microwaves by clouds and precipitation in radar meteorology [1], and with the net radiative impact of clouds on the global climate [2,3]. Particulate radiation is of primary importance in the area of fuel combustion as is the case in coal furnaces, fluidized beds, and luminous flames. For the latter, soot particles are responsible for the luminous emission from the flame. The use of water sprays for fire suppression becomes again the primary fire extinguishing fire agent since the production of Halon has been prohibited by international agreement. Light scattering can also be used as diagnostic technique for measurement and visualization in gases and liquids seeded by small particles.

Radiation in particulate media can be approached by a continuum treatment leading to the statement of a radiative energy balance, known as the radiative transfer equation (RTE) [4], by the direct Monte-Carlo method [5], or by the multilayer method [6]. In the continuum approach, it is often assumed that the average interparticle spacing is large compared with the wavelength of the radiation (the criterion $c/\lambda > 0.5$ is generally retained) for the applicability of the independent theory [7]. By applying this theory, the radiative properties of the packed bed may be related to the properties of an individual particle, neglecting interactions between the particles. For example, Park et al. [8] and Kim et al. [9] used the independent theory to model two-phase radiation in high-porosity systems. The authors considered the mixture of the gas and particles as a gray, emitting, absorbing, and scattering two-phase medium. Gas scattering is neglected and the particles are assumed to be large (geometric range, $\chi > 5$), opaque and diffusely reflecting spheres. Singh and Kaviany [10] compare, for

* Corresponding author. Tel.: +33-04-9110-6931; fax: +33-04-9110-6969.

E-mail address: berni@iusti.univ-mrs.fr (B. Porterie).

0017-9310/02/$ - see front matter
PII: S0017-9310(02)00007-8

Nomenclature

A_k	specific wetted area of phase k ($A_k = \alpha_k \sigma_k$) (m^{-1})
c	average interparticle clearance (m)
c_p	specific heat (J kg^{-1} K^{-1})
d	particle diameter (m)
g	weighting function
G	average incident radiation (W m^{-2})
h	conductive heat transfer coefficient (W m^{-2} K^{-1})
L	radiative intensity (W m^{-2} sr^{-1})
L_x, L_y, L_z	dimensions of the enclosure in the x-, y-, and z-directions (m)
$\mathbf{n}$	unit surface normal (pointing away from surface into the medium)
n_k	number of particles of particle phase k per unit volume (m^{-3})
N	number of particle phases
P_m	Legendre polynomials
P_k	total number of particles of particle phase k
$\mathbf{q}_c$	conductive heat flux (W m^{-2})
$\mathbf{q}_r$	radiative heat flux (W m^{-2})
s_{pk}	surface of a particle of particle phase k (m^2)
T	temperature (K)
v_{pk}	volume of a particle of particle phase k (m^3)
x, y, z	Cartesian coordinates
α	phase volume fraction
β	extinction coefficient (m^{-1})
δ_k	mean free path length for radiation of particle phase k (m)
ε	emissivity
θ	polar angle, measured from the z-axis
λ	wavelength (m), thermal conductivity (W m^{-1} K^{-1})
μ, η, ξ	direction cosines
ρ	density (kg m^{-3})
σ	Stefan–Boltzmann constant (W m^{-2} K^{-4})
σ_k	surface area to volume ratio of particle phase k (m^{-1})
τ	optical thickness
Φ	phase function
φ	azimuthal angle, in the x–y plane, measured from the x-axis
χ	size parameter ($= \pi d_k/\lambda$)
ψ	scattering angle between incident and scattering directions
ω	albedo
$\mathbf{\Omega}$	directional vector of radiative intensity

Superscripts

w, e, s, n, b, f	control-volume faces
m	discrete direction

Subscripts

g	gas phase
k	particle phase k
p	particle
w	wall value
b	blackbody value

Symbols

$\Delta x, \Delta y, \Delta z$	cell dimensions
ΔV	cell volume
$\langle\rangle$	weighted-average value
$+, -$	into positive or negative x-directions
$*$	non-dimensional value

large particles, the independent theory with the direct Monte-Carlo method and with experiments, assuming a radiatively non-participating gas phase. They found that the independent theory fails for systems with low porosity for both opaque and transparent particles even when the criterion $c/\lambda > 0.5$ is satisfied. On the other hand, at high porosity ($\alpha_g \geqslant 0.992$), it gives good predictions. The authors attribute this failure to two distinct dependent scattering effects. The first is due to the multiple scattering which increases the effective scattering and absorption cross-sections of the particles and the second is due to the transportation of radiation through transparent and semi-transparent particles. In a next paper [11], these same authors take into account these two phenomena while retaining the continuum approach. The first dependence is taken into account by scaling the optical thickness obtained from the independent theory to give the dependent properties of the particulate medium. Transportation effects are modeled by introducing a phase function which depends on the exit point of the sphere and of the number of internal reflections. A better agreement is obtained.

The general approach proposed in the present study is based on the application of the formal averaging method [12] to the RTE for a multiphase medium composed of a gas phase and large opaque spherical particles. The resulting multiphase radiative transfer equation (MRTE) is validated by comparing with the Chen and Churchill experiment and the results provided by the direct Monte-Carlo method. For such one-dimensional comparison, the gas is assumed to be radiatively non-participating (i.e., transparent) and absorbing, diffusely scattering particles are considered. The

discrete ordinates method is used to solve the MRTE. After applying the formal averaging procedure to the energy equations for each phase, the coupling with the MRTE is considered to study combined conductive and radiative transfers in a three-dimensional enclosure which is differentially heated or which contains a high-temperature source (simulating fire in a room or combustion process). In this study, gas and particles are at rest and emission, absorption, and scattering are considered for all phases. Spherical particles are assumed to be thermally thick (uniform temperature distribution inside the particle). The DOM is also used to solve the MRTE while the finite-volume method and the fourth-order Runge–Kutta algorithm are used for solving the energy equation for the gas and particle phases, respectively. The influence of several parameters, such as particle-phase specific surface, gas scattering phase function, particle and wall emissivity is examined.

2. Analysis

In the present approach, the multiphase medium is composed of a gas phase and particles of various kinds. In a small control volume V, N particle phases coexist with a gas phase. Each particle phase consists of particles having the same geometrical (e.g., shape, size, and arrangement), thermophysical, and radiative properties, providing in this way the same response to external constraints. The volume fraction of phase k is defined as $\alpha_k = V_k/V$, where V_k is the volume occupied by phase k in volume V. In the same way, the fractional porosity, also called the void fraction, is defined as $\alpha_g = V_g/V$. From these definitions, we have

$$\alpha_g + \sum_{k=1}^{N} \alpha_k = 1. \tag{1}$$

The formal averaging method used in the present paper was first introduced by Anderson and Jackson [12] and used later by Gough and Zwarts [13] in a slightly different form. This consists in replacing point variables such as the gas temperature, the radiative intensity, or the temperature of particle matter at a specified point, by local mean variables obtained by averaging the local variables over regions which are large enough to contain many particles but small compared with the scale of macroscopic variations from point to point in the system. Following Anderson and Jackson [12], we shall define a weighting function which depends solely on spatial coordinates. Some definitions and approximations are needed for the derivation of macroscopic equations using the formal averaging method.

Let a weighting function $g(r)$, defined for $r > 0$, with the following mathematical properties:

1. $g(r) \geqslant 0$ for all r, and g decreases monotonically with increasing r,
2. $g(r)$ possesses derivatives $g^n(r)$ of all orders for each values of r,
3. $\int_{V_\infty} g^n(r)\,\mathrm{d}V = 1$ exists for all values of n, where r denotes the distance from a point in a three-dimensional space, and V_∞ represents the whole space, and
4. $g(r)$ is normalized so that $\int_{V_{g\infty}} g^n(r)\,\mathrm{d}V = 1$.

The local mean void fraction, α_g, at location $\mathbf{x}$ and time t is defined as

$$\alpha_g(\mathbf{x};t) = \int_{V_{g\infty}} g(|\mathbf{x}-\mathbf{y}|)\,\mathrm{d}V_y \tag{2}$$

where $V_{g\infty}$ is the volume occupied by the gas phase at time t and $\mathrm{d}V_y$ is an elemental volume in the neighborhood of point $\mathbf{y}$. In a similar manner, the local mean volume fraction of particle phase k is defined by

$$\alpha_k(\mathbf{x};t) = \int_{V_{k\infty}} g(|\mathbf{x}-\mathbf{y}|)\,\mathrm{d}V_y. \tag{3}$$

Local mean values of any gas property, a_g, and any particle-phase property, a_k, are given by

$$\alpha_g\langle a_g\rangle(\mathbf{x};t) = \int_{V_{g\infty}} a_g(\mathbf{y};t)g(|\mathbf{x}-\mathbf{y}|)\,\mathrm{d}V_y, \tag{4}$$

$$\alpha_k\langle a_k\rangle(\mathbf{x};t) = \int_{V_{k\infty}} a_k(\mathbf{y};t)g(|\mathbf{x}-\mathbf{y}|)\,\mathrm{d}V_y. \tag{5}$$

2.1. Multiphase radiative transfer equation

The local instantaneous equation of radiative transfer for an emitting–absorbing–scattering gray continuum may be written [4]

$$\nabla\cdot\left(L_g^{\Omega}\boldsymbol{\Omega}\right) + \beta_g L_g^{\Omega} = (1-\omega_g)\beta_g L_b(T_g) + \frac{\omega_g\beta_g}{4\pi} \times \int_{4\pi} L_g^{\Omega'}\Phi_g^{\Omega\Omega'}\,\mathrm{d}\Omega'. \tag{6}$$

Multiplying both sides by the weighting function and integrating over the whole region occupied by gas, we get

$$\int_{V_{g\infty}} g\left\{\nabla\cdot\left(L_g^{\Omega}\boldsymbol{\Omega}\right) + \beta_g L_g^{\Omega}\right\}\mathrm{d}V_y = (1-\omega_g)\beta_g\int_{V_{g\infty}} gL_b(T_g)\,\mathrm{d}V_y + \frac{\omega_g\beta_g}{4\pi} \times \int_{V_{g\infty}} g\left[\int_{4\pi} L_g^{\Omega'}\Phi_g^{\Omega\Omega'}\,\mathrm{d}\Omega'\right]\mathrm{d}V_y, \tag{7}$$

where the weighting function g has been assumed to decrease rapidly enough for integration to be done over

a volume containing a large number of particles but small enough compared with the dimensions of the problem for the physical characteristics of the particulate and gas phases (i.e., ω_g, β_g, ε_k, and σ_k) to be assumed constant.

Using mathematical theorems given in Appendix A and permuting integrals in the last term of the right-hand side yield

$$\nabla\cdot\left[\alpha_g\left\langle L_g^{\Omega}\right\rangle\mathbf{\Omega}\right]+\sum_{k=1}^{N}\sum_{p=1}^{P_k}\int_{s_{pk}} gL_g^{\Omega}\mathbf{\Omega}\cdot\mathbf{n}_g\,ds+\alpha_g\beta_g\left\langle L_g^{\Omega}\right\rangle = \alpha_g(1-\omega_g)\beta_g\langle L_b(T_g)\rangle+\frac{\alpha_g\omega_g\beta_g}{4\pi}\int_{4\pi}\left\langle L_g^{\Omega'}\right\rangle\Phi_g^{\Omega\Omega'}\,d\Omega'. \tag{8}$$

The second term of the left-hand side of this equation corresponds to the interactions between the gas and the particle phases. To evaluate this term we consider an absorbing, emitting and scattering particle of volume v_{pk} and surface s_{pk} and on this surface, a surface-area element ds described by the polar and azimuthal angles, θ and φ. The azimuthal direction corresponds to direction $\mathbf{\Omega}$.

At this stage, the assumption of large (geometric range) particles is used. Diffraction is neglected and treated as transmission, as usually done in heat transfer problems [4]. To carry out integration, the sphere surface is divided into two:

- s_{pk}^{+} , $\theta\in[0,\pi/2]$,
- s_{pk}^{-} , $\theta\in[\pi/2;\pi]$.

Over s_{pk}^{+}: The energy passing through a surface element in direction $\mathbf{\Omega}$ is equal to the energy emitted by the particle in direction $\mathbf{\Omega}$ plus the energy reflected by its surface in direction $\mathbf{\Omega}$. This balance leads to the relation

$$L_g^{\Omega}=\varepsilon_k L_b(T_k)+E_s^{\Omega}. \tag{9}$$

The energy reflected (or scattered) per unit of surface and of solid angle of direction $\mathbf{\Omega}'$ in direction $\mathbf{\Omega}$ is equal to $(1-\varepsilon_k)L_g^{\Omega'}\Phi_k^{\Omega\Omega'}/4\pi$.

By integrating over all the incident directions, we obtain

$$E_s^{\Omega}=\int_{4\pi}(1-\varepsilon_k)L_g^{\Omega'}\frac{\Phi_k^{\Omega\Omega'}}{4\pi}\,d\Omega'. \tag{10}$$

It follows that

$$L_g^{\Omega}=\varepsilon_k L_b(T_k)+\int_{4\pi}(1-\varepsilon_k)L_g^{\Omega'}\frac{\Phi_k^{\Omega\Omega'}}{4\pi}\,d\Omega'. \tag{11}$$

Over s_{pk}^{-}: All the energy which passes through a surface element in direction $\mathbf{\Omega}$ is either absorbed by the particle or reflected by this particle in a direction $\mathbf{\Omega}'$.

The relation sought is thus written as

$$\begin{aligned}\int_{s_{pk}} gL_g^{\Omega}\mathbf{\Omega}\cdot\mathbf{n}_g\,ds &= \int_{s_{pk}^{+}} g\varepsilon_k L_b(T_k)\mathbf{\Omega}\cdot\mathbf{n}_g\,ds\\ &+\int_{s_{pk}^{+}} g\left[\int_{4\pi}(1-\varepsilon_k)L_g^{\Omega'}\frac{\Phi_k^{\Omega\Omega'}}{4\pi}\,d\Omega'\right]\mathbf{\Omega}\cdot\mathbf{n}_g\,ds\\ &+\int_{s_{pk}^{-}} gL_g^{\Omega}\mathbf{\Omega}\cdot\mathbf{n}_g\,ds.\end{aligned} \tag{12}$$

Assuming the weighting function and the radiative intensity vary little at the particle surface, we have

$$\int_{s_{pk}^{-}} gL_g^{\Omega}\mathbf{\Omega}\cdot\mathbf{n}_g\,ds=\frac{1}{4}s_{pk}g_{pk}L_g^{\Omega} \tag{13}$$

and

$$\int_{s_{pk}^{+}} gL_g^{\Omega}\mathbf{\Omega}\cdot\mathbf{n}_g\,ds=-\frac{1}{4}\varepsilon_k s_{pk}g_{pk}L_b(T_k) -\frac{1-\varepsilon_k}{16\pi}s_{pk}g_{pk}\int_{4\pi}L_g^{\Omega'}\Phi_k^{\Omega\Omega'}\,d\Omega'. \tag{14}$$

By summing over all the particles of phase k, it follows (Appendix A):

$$\sum_{p=1}^{P_k}\int_{s_{pk}^{-}} gL_g^{\Omega}\mathbf{\Omega}\cdot\mathbf{n}_g\,ds\approx\frac{\alpha_k\sigma_k}{4}\left\langle L_g^{\Omega}\right\rangle \tag{15}$$

and

$$\int_{s_{pk}^{+}} gL_g^{\Omega}\mathbf{\Omega}\cdot\mathbf{n}_g\,ds\approx-\frac{\alpha_k\varepsilon_k\sigma_k}{4}\langle L_b(T_k)\rangle -\frac{\alpha_k(1-\varepsilon_k)\sigma_k}{16\pi}\times\int_{4\pi}\left\langle L_g^{\Omega'}\right\rangle\Phi_k^{\Omega\Omega'}\,d\Omega'. \tag{16}$$

The MRTE can finally be written as

$$\begin{aligned}\nabla\cdot\left[\alpha_g\left\langle L_g^{\Omega}\right\rangle\mathbf{\Omega}\right]+\sum_{k=1}^{N}\frac{\alpha_k\sigma_k}{4}\left\langle L_g^{\Omega}\right\rangle+\alpha_g\beta_g\left\langle L_g^{\Omega}\right\rangle &= \alpha_g(1-\omega_g)\beta_g\langle L_b(T_g)\rangle+\sum_{k=1}^{N}\frac{\alpha_k\varepsilon_k\sigma_k}{4}\langle L_b(T_k)\rangle\\ &+\frac{\alpha_g\omega_g\beta_g}{4\pi}\int_{4\pi}\left\langle L_g^{\Omega'}\right\rangle\Phi_g^{\Omega\Omega'}\,d\Omega'+\sum_{k=1}^{N}\frac{\alpha_k(1-\varepsilon_k)\sigma_k}{16\pi}\\ &\times\int_{4\pi}\left\langle L_g^{\Omega'}\right\rangle\Phi_k^{\Omega\Omega'}\,d\Omega'.\end{aligned} \tag{17}$$

To solve the MRTE, boundary conditions at the walls are needed. The exchanges between the walls and the medium will be assumed to occur solely via the gas. Only diffuse gray wall conditions will be used in this paper:

$$\left\langle L_{\mathrm{g}}^{\Omega}\right\rangle = \varepsilon_{\mathrm{w}}\langle L_{\mathrm{b}}(T_{\mathrm{w}})\rangle + \frac{1-\varepsilon_{\mathrm{w}}}{\pi}\int_{\mathbf{\Omega}'\cdot\mathbf{n}_{\mathbf{w}}<0}\left\langle L_{\mathrm{g}}^{\Omega'}\right\rangle|\mathbf{\Omega}'\cdot\mathbf{n}_{\mathbf{w}}|\,\mathrm{d}\Omega'. \tag{18}$$

To determine the divergence of the radiative flux in the gas phase given by

$$\langle\mathbf{q}_{\mathrm{rg}}\rangle = \int_{4\pi}\left\langle L_{\mathrm{g}}^{\Omega}\right\rangle\mathbf{\Omega}\,\mathrm{d}\Omega. \tag{19}$$

The MRTE is integrated over all the directions, that is, for $\mathbf{\Omega}$ varying from 0 to 4π. Examination of the left-hand member of the MRTE shows that the extinction coefficients include an absorbed part and a part scattered from the direction $\mathbf{\Omega}$ into another direction $\mathbf{\Omega}'$. By summing over all the directions the scattered part is cancelled with the last two terms of the right-hand member of the MRTE such that only the absorbed part remains non-zero in the equation sought.

$$\begin{aligned}\nabla\cdot[\alpha_{\mathrm{g}}\langle\mathbf{q}_{\mathrm{rg}}\rangle] &= 4\pi\alpha_{\mathrm{g}}(1-\omega_{\mathrm{g}})\beta_{\mathrm{g}}\langle L_{\mathrm{b}}(T_{\mathrm{g}})\rangle - \alpha_{\mathrm{g}}(1-\omega_{\mathrm{g}})\beta_{\mathrm{g}}\int_{4\pi}\left\langle L_{\mathrm{g}}^{\Omega}\right\rangle\mathrm{d}\Omega \\ &\quad + \sum_{k=1}^{N}\pi\alpha_k\sigma_k\varepsilon_k\langle L_{\mathrm{b}}(T_k)\rangle - \sum_{k=1}^{N}\frac{\alpha_k\sigma_k\varepsilon_k}{4}\int_{4\pi}\left\langle L_{\mathrm{g}}^{\Omega}\right\rangle\mathrm{d}\Omega.\end{aligned} \tag{20}$$

2.2. Coupling with conduction

Since the temperature distribution is assumed to be uniform inside the particle (thermally thin assumption), the conduction in the gas phase is only considered. An evaluation of Mazza et al. [14] suggested that a good criterion to ignore finite particle conductivity effects is $\lambda_k/\lambda_{\mathrm{g}} > 30$. In the present work, all phases are assumed to be at rest. Opaque particles are considered.

On the other hand, the pseudo-transient method is used to solve the energy equations. For steady problems, an alternative to the solution of the algebraic equations produced by discretizing the steady problem is to construct an equivalent unsteady problem and to march the transient solution until the steady-state is reached. Time then plays the role of an iteration parameter. This approach to the steady-state is found to be more rapid in all parts of the computational domain. Since the transient solution is not of interest, time-step is chosen to minimize the number of time-steps to convergence and to maintain the accuracy and the stability of the evolving equations. This is the motivation for the pseudo-transient method.

Before applying the formal averaging method, the point energy equations for the gas and particle phases and the associated jump condition at the particle–gas interface are obtained from the method proposed by Delhaye [15] by considering a small control volume containing both the gas phase and one particle phase (Fig. 1). The heat balance equation over this volume yields

$$\begin{aligned}&\int_{V_{\mathrm{g}}}\rho_{\mathrm{g}}c_{\mathrm{pg}}\frac{\partial T_{\mathrm{g}}}{\partial t}\,\mathrm{d}V + \int_{V_k}\rho_k c_{\mathrm{pk}}\frac{\partial T_k}{\partial t} \\ &\quad = -\int_{A_{\mathrm{g}}}(\mathbf{q}_{\mathrm{cg}}+\mathbf{q}_{\mathrm{rg}})\cdot\mathbf{n}_{\mathrm{g}}\,\mathrm{d}s - \int_{A_k}\mathbf{q}_{\mathrm{r}k}\cdot\mathbf{n}_{\mathbf{k}}\,\mathrm{d}s.\end{aligned} \tag{21}$$

Introducing the fluxes at the gas–particle interface and applying the Gauss theorem, we obtain

$$\begin{aligned}&\int_{V_{\mathrm{g}}}\rho_{\mathrm{g}}c_{\mathrm{pg}}\frac{\partial T_{\mathrm{g}}}{\partial t}\,\mathrm{d}V + \int_{V_k}\rho_k c_{\mathrm{pk}}\frac{\partial T_k}{\partial t} + \int_{V_{\mathrm{g}}}\nabla\cdot(\mathbf{q}_{\mathrm{cg}}+\mathbf{q}_{\mathrm{rg}})\,\mathrm{d}V \\ &\quad + \int_{V_k}\nabla\cdot\mathbf{q}_{\mathrm{r}k}\,\mathrm{d}V = \int_{A_I}\{(\mathbf{q}_{\mathrm{cg}}+\mathbf{q}_{\mathrm{rg}})\cdot\mathbf{n}_{\mathrm{g}} + \mathbf{q}_{\mathrm{r}k}\cdot\mathbf{n}_{\mathbf{k}}\}\,\mathrm{d}s.\end{aligned} \tag{22}$$

Providing that this equation is satisfied at every point and every time, the local instantaneous equations are:

- Gas phase:

$$\rho_{\mathrm{g}}c_{\mathrm{pg}}\frac{\partial T_{\mathrm{g}}}{\partial t} = -\nabla\cdot\mathbf{q}_{\mathrm{rg}} - \nabla\cdot\mathbf{q}_{\mathrm{cg}}. \tag{23}$$

- Particle phase ($k\in\{1,N\}$):

$$\rho_k c_{\mathrm{pk}}\frac{\partial T_k}{\partial t} = -\nabla\cdot\mathbf{q}_{\mathrm{r}k}. \tag{24}$$

- Interface ($k\in\{1,N\}$):

$$(\mathbf{q}_{\mathrm{cg}}+\mathbf{q}_{\mathrm{rg}})\cdot\mathbf{n}_{\mathrm{g}} + \mathbf{q}_{\mathrm{r}k}\cdot\mathbf{n}_{\mathbf{k}} = \mathbf{0}, \tag{25}$$

where

$$\mathbf{q}_{\mathrm{cg}} = -\lambda_{\mathrm{g}}\nabla T_{\mathrm{g}}, \tag{26}$$

$$\mathbf{q}_{\mathrm{rg}} = \int_{4\pi}L_{\mathrm{g}}^{\Omega}\mathbf{\Omega}\,\mathrm{d}\Omega. \tag{27}$$

The use of the formal averaging method gives

$$\begin{aligned}\alpha_{\mathrm{g}}\rho_{\mathrm{g}}c_{\mathrm{pg}}\frac{\partial\langle T_{\mathrm{g}}\rangle}{\partial t} &= -\nabla\cdot[\alpha_{\mathrm{g}}(\langle\mathbf{q}_{\mathrm{rg}}\rangle + \langle\mathbf{q}_{\mathrm{cg}}\rangle)] \\ &\quad - \sum_{k=1}^{N}\sum_{p=1}^{P_k}\int_{s_{pk}}g(\mathbf{q}_{\mathrm{rg}}+\mathbf{q}_{\mathrm{cg}})\cdot\mathbf{n}_{\mathrm{g}}\,\mathrm{d}s,\end{aligned} \tag{28}$$

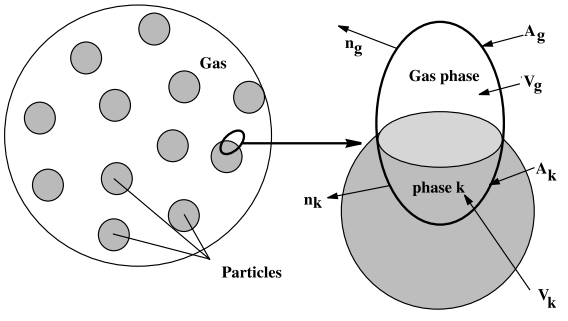

Fig. 1. Sketch of a control volume.

$$\alpha_k \rho_k c_{pk} \frac{\partial \langle T_k \rangle}{\partial t} = -\nabla \cdot [\alpha_k \langle \mathbf{q}_{rk} \rangle] - \sum_{p=1}^{P_k} \int_{s_{pk}} g \mathbf{q}_{rk} \cdot \mathbf{n}_k \, \mathrm{d}s. \tag{29}$$

Since for opaque particles, $\nabla \cdot [\alpha_k \langle \mathbf{q}_{rk} \rangle] = 0$, using the interface condition we can write

$$\alpha_k \rho_k c_{pk} \frac{\partial \langle T_k \rangle}{\partial t} = \sum_{p=1}^{P_k} \int_{s_{pk}} g(\mathbf{q}_{rg} + \mathbf{q}_{cg}) \cdot \mathbf{n}_g \, \mathrm{d}s. \tag{30}$$

The conductive flux term can be developed (see Appendix A):

$$\begin{aligned} \alpha_g \langle \mathbf{q}_{cg} \rangle &= -\lambda_g \langle \nabla T_g \rangle \\ &= -\lambda_g \nabla (\alpha_g \langle T_g \rangle) - \sum_{k=1}^{N} \sum_{p=1}^{P_k} \int_{s_{pk}} g T_g \mathbf{n}_g \, \mathrm{d}s \end{aligned} \tag{31}$$

which, assuming that the gas temperature at the surface of a particle of phase k is constant, reduces to

$$\alpha_g \langle \mathbf{q}_{cg} \rangle = -\lambda_g \nabla (\alpha_g \langle T_g \rangle). \tag{32}$$

These exchanges will be assumed to be constant over all the gas–particle interface of a particle of phase k such that

$$\sum_{p=1}^{P_k} \int_{s_{pk}} g \mathbf{q}_{cg} \cdot \mathbf{n}_g \, \mathrm{d}s = A_k h_k (\langle T_g \rangle - \langle T_k \rangle). \tag{33}$$

Since the particles are at rest, $h_k = \lambda_g Nu_k / d_k$ is calculated by assuming Nusselt number equal to 2.

Radiative exchanges at the interface may be expressed by integrating Eq. (12) over all directions and by summing over all the particles of phase k,

$$\begin{aligned} \sum_{p=1}^{P_k} \int_{s_{pk}} g \mathbf{q}_{rg} \cdot \mathbf{n}_g \, \mathrm{d}s &= -\pi \alpha_k \sigma_k \varepsilon_k \langle L_b(T_k) \rangle \\ &\quad + \frac{\alpha_k \sigma_k \varepsilon_k}{4} \int_{4\pi} \left\langle L_g^{\Omega} \right\rangle \mathrm{d}\Omega. \end{aligned} \tag{34}$$

It follows that the heat equations for the gas phase and the particle phases are written as

$$\begin{aligned} \alpha_g \rho_g c_{pg} \frac{\partial \langle T_g \rangle}{\partial t} &= \lambda_g \triangle [\alpha_g \langle T_g \rangle] + (1 - \omega_g) \beta_g \alpha_g \langle G \rangle \\ &\quad - 4 \alpha_g (1 - \omega_g) \beta_g \sigma \left\langle T_g^4 \right\rangle \\ &\quad - \sum_{k=1}^{N} A_k h_k (\langle T_g \rangle - \langle T_k \rangle), \end{aligned} \tag{35}$$

$$\begin{aligned} \alpha_k \rho_k c_{pk} \frac{\partial \langle T_k \rangle}{\partial t} &= \frac{\alpha_k \sigma_k}{4} \varepsilon_k \langle G \rangle - \alpha_k \sigma_k \varepsilon_k \sigma \left\langle T_k^4 \right\rangle \\ &\quad + A_k h_k (\langle T_g \rangle - \langle T_k \rangle), \end{aligned} \tag{36}$$

where the average incident radiation is

$$G = \int_{4\pi} L(\mathbf{\Omega}) \, \mathrm{d}\Omega. \tag{37}$$

3. Numerical resolution

To solve the MRTE the discrete ordinates method (DOM) is used [16]. DO solutions can be obtained using S_n approximations. This means that radiation calculations are based on solving the RTE in $M = n(n+2)$ discrete solutions to which a set of weights is attached. In the current study, the ordinate directions and quadratic weighting factors (μ_m, η_m, ξ_m, and w_m) have been taken from the well-known TWOTRAN II code [17]. The MRTE is integrated over a control volume given in Fig. 2. By setting

$$\begin{aligned} S_p^m &= \sum_{k=1}^{N} \frac{\alpha_k \sigma_k}{4} \varepsilon_k \langle L_b(T_k) \rangle + \alpha_g \left\langle (1 - \omega_g) \beta_g L_b(T_g) \right\rangle \\ &\quad + \sum_{k=1}^{N} \frac{\alpha_k \sigma_k (1 - \varepsilon_k)}{16\pi} \sum_{m'=1}^{M} \left\langle L_g^{m'p} \right\rangle \Phi_g^{mm'} \omega_{m'} \\ &\quad + \frac{\alpha_g \omega_g \beta_g}{4\pi} \sum_{m'=1}^{M} \left\langle L_g^{m'p} \right\rangle \Phi_g^{mm'} \omega_{m'}. \end{aligned} \tag{38}$$

The discretized MRTE is for $m \in \{1, M\}$:

$$\begin{aligned} &\mu_m \Delta y \Delta z \left[\alpha_g^e \langle L_g^{me} \rangle - \alpha_g^w \left\langle L_g^{mw} \right\rangle \right] + \eta_m \Delta x \Delta z \left[\alpha_g^n \left\langle L_g^{mn} \right\rangle \right. \\ &\quad \left. - \alpha_g^s \left\langle L_g^{ms} \right\rangle \right] + \xi_m \Delta x \Delta y \left[\alpha_g^f \left\langle L_g^{mf} \right\rangle - \alpha_g^b \left\langle L_g^{mb} \right\rangle \right] \\ &\quad + \beta_T \left\langle L_g^{mp} \right\rangle \Delta V = S_p^m \Delta V, \end{aligned} \tag{39}$$

where $\beta_T = \sum_{k=1}^{N} \alpha_k \sigma_k / 4 + \alpha_g \beta_g$. The variable weighted scheme of Lathrop [18] is used to relate the facial intensities at the boundary of control volume to the cell center intensity

$$\begin{aligned} L_g^{mp} &= X L_g^{me} + (1 - X) L_g^{mw} = Y L_g^{mn} + (1 - Y) L_g^{ms} \\ &= Z L_g^{mf} + (1 - Z) L_g^{mb} \end{aligned} \tag{40}$$

The expressions of X, Y and Z are given by

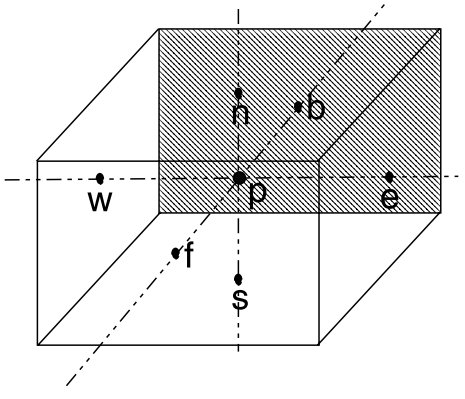

Fig. 2. Schematic of grid points and control volume for the computation.

$$1 - X = \frac{\beta_m \gamma_m}{\alpha_m(2\beta_m + 2\gamma_m + \beta_m\gamma_m)} \quad \text{and} \quad X = \max[X; 0.5], \tag{41}$$

$$1 - Y = \frac{\alpha_m \gamma_m}{\beta_m(2\alpha_m + 2\gamma_m + \alpha_m\gamma_m)} \quad \text{and} \quad Y = \max[Y; 0.5], \tag{42}$$

$$1 - Z = \frac{\beta_m \alpha_m}{\gamma_m(2\beta_m + 2\alpha_m + \beta_m\alpha_m)} \quad \text{and} \quad Z = \max[Z; 0.5], \tag{43}$$

where

$$\alpha_m = \frac{\beta_T \Delta x}{\mu_m}, \quad \beta_m = \frac{\beta_T \Delta y}{\eta_m}, \quad \gamma_m = \frac{\beta_T \Delta z}{\xi_m}. \tag{44}$$

The luminance value at the center of the cell is given by

$$\begin{aligned} L_g^{mp} = \{&C_x[A_e + A_w]L_g^{mw} + C_y[A_n + A_s]L_g^{ms} \\ &+ C_z[A_f + A_b]L_g^{mb} + S_p^m \Delta V\}/\{C_x\alpha_g^e + C_y\alpha_g^n \\ &+ C_z\alpha_g^f + \beta_T \Delta V\} \end{aligned} \tag{45}$$

with

$$\begin{aligned} &C_x = \frac{\mu_m \Delta y \Delta z}{X}, \quad C_y = \frac{\eta_m \Delta x \Delta z}{Y}, \quad C_z = \frac{\xi_m \Delta x \Delta y}{Z}, \\ &A_e = \alpha_g^e(1 - X), \quad A_w = \alpha_g^w X, \quad A_n = \alpha_g^n(1 - Y), \\ &A_s = \alpha_g^s Y, \\ &A_f = \alpha_g^f(1 - Z) \text{ and } A_b = \alpha_g^b Z. \end{aligned} \tag{46}$$

Later in the presentation the $S-4$ to $S-16$ will be applied. By solving the MRTE, the average incident radiation G field can be obtained.

The energy equation for particle phase k is an ordinary differential equation which is solved with the fourth-order Runge–Kutta scheme.

For the gas phase, the energy equation is a partial differential equation which is discretized on an uniform grid using a finite-volume procedure along with a second-order backward Euler scheme for time integration. Diffusion terms are approximated using a second-order central difference scheme. The resulting system of linear algebraic equations is then solved iteratively using the tri-diagonal matrix algorithm (TDMA) [19].

The present study concerns only steady cases. The thermal equilibrium which characterizes them is obtained by an iterative process. The process is repeated until the following convergence criterion is satisfied for the particle-phase temperature

$$\max\left(|T_k^{n+1} - T_k^n|/T_k^n\right) \leqslant 0.0001. \tag{47}$$

For the results reported, convergence was excellent, with no need for any relaxation. A fully converged run, using the S-12 approximation, the $20 \times 11 \times 11$ grid, and a particle-phase specific surface of 3 m^{-1}, required 54 sweeps with a total CPU time of 30 mn on a 1 GHz Athlon PC.

4. Results and discussion

4.1. Comparison of METR with Monte-Carlo simulations and Chen and Churchill experiments

Results predicted from our model are compared to the experimental results of Chen and Churchill [20] and to the results of the Monte-Carlo simulations for one-dimensional beds of large, opaque, gray and spherical particles. For this we will use experimental situations or numerical simulations by the Monte-Carlo method presented in [10]. In the present calculations, $S-16$ approximations are used.

In the experiments of Chen and Churchill, radiant transmission was measured through isothermal beds of steel spheres ($d_k = 4.7625$ mm, $\alpha_k = 0.4$) using an emissivity of 0.4. Particles are considered to be reflecting, absorbing, and non-emitting. In our model and in the independent model used by Singh and Kaviany [10], diffusely reflecting spheres are considered while diffraction is neglected. For diffuse scattering, the phase function is given by [4]

$$\Phi_k^{\Omega\Omega'} = \frac{8}{3\pi}(\sin\psi - \psi\cos\psi) \tag{48}$$

This phase function is represented in Fig. 3. The transmittance through such a medium is represented in Fig. 4. MRTE predictions are in better agreement with the experimental results. As suggested by Chen and Churchill [20], the deviations can be explained by the uncertainties concerning the emissivity of the steel spheres as a result of its temperature dependency and the presence of an oxide coating [20]. In fact the first couple of layers might be at a higher temperature than the rest of the bed because of their proximity to the source [10].

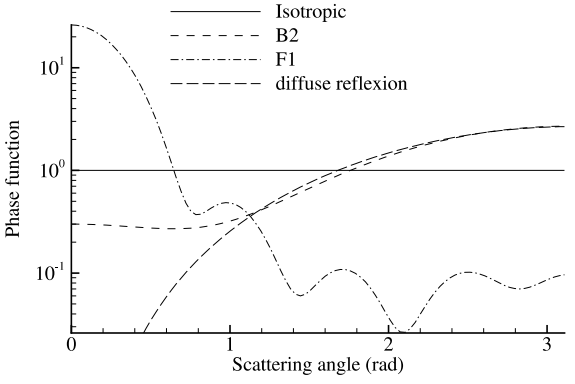

Fig. 3. Scattering phase functions.

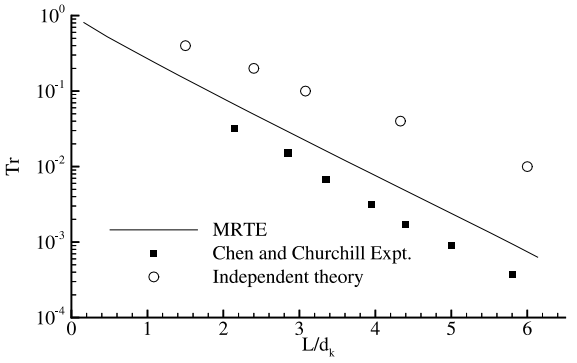

Fig. 4. Transmittance from a bed of steel spheres: comparison of the MRTE predictions with the Chen and Churchill experiments.

A comparison with Monte-Carlo simulations is also presented assuming diffusely reflecting, absorbing, and non-emitting spheres with an emissivity of 0.3. The studied configurations correspond, for the couple (α_g, d_k), to the following values: (0.476,1.0), (0.732,0.8), (0.935,0.5), (0.992,0.25). According to the independent theory the following systems are exactly equivalent [10]. In Fig. 5 the transmittances in these media calculated by the MRTE and by the Monte-Carlo method are represented versus the independent optical thickness $\tau_{ind} = 1.5(1-\alpha_g)x/d_k$. This quantity τ_{ind} is obtained from the definition of the optical thickness of an absorbing and emitting medium assuming a mono-size, large (diffraction can thus be neglected; i.e., the extinction efficiency is equal to 1), uniformly distributed particles [10]. The results supplied by the independent theory are also plotted. The results supplied by the MRTE are in very good agreement with those obtained by the Monte-Carlo method. The theory of independent scattering gives results in good agreement with Monte-Carlo simulations only for high porosity [10].

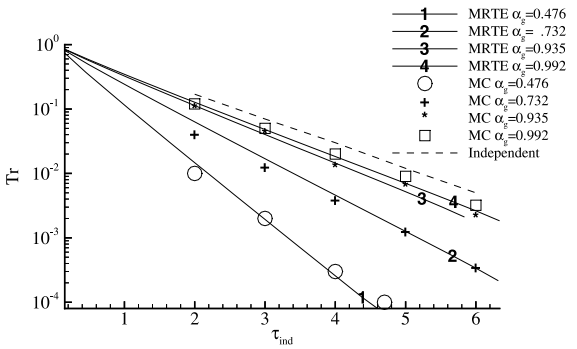

Fig. 5. Transmittance from a packed bed: comparison of the MRTE predictions with the Monte-Carlo direct simulation and independent theory.

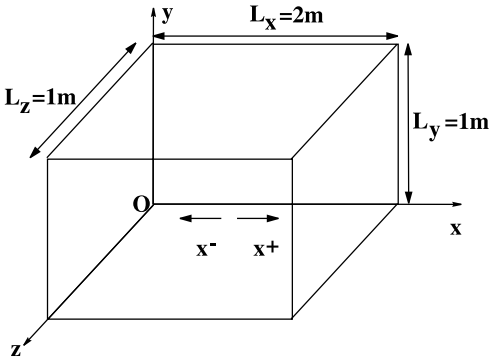

Fig. 6. Schematic diagram of the enclosure.

4.2. Sensitivity study

4.2.1. Problem description

We consider here the coupling of radiation and conduction in a three-dimensional rectangular enclosure (Fig. 6). The dimensions of the enclosure are 2 m × 1 m × 1 m. Different grid sizes were tested to ensure that the solution was independent of the grid density. A grid size of 20 × 11 × 11 is used for all calculations. The west wall ($x = 0$) is at 1000 K with the remaining walls maintained at 300 K. The enclosure walls are assumed to be black ($\varepsilon_w = 1$). In this sensitivity study a single particle phase is taken into account ($N = 1$), for if we consider a set of N particle phases, it is always possible to find an equivalent particle phase whose properties

$$\alpha_{eq} = \sum_{k=1}^{N} \alpha_k, \quad \sigma_{eq} = \frac{\sum_{k=1}^{N} \alpha_k \sigma_k}{\alpha_{eq}}$$

will give identical results. This assertion is only possible if the particles which make up the particle phases have the same emissivity. Both phases whose geometrical and thermophysical properties for both phases are given in Table 1 participate in absorption, emission and scattering of radiation. The optical thickness of the multiphase medium and of the particle phase in the direction **i** may be defined as

$$\tau_i = \left(\alpha_g \beta_g + \frac{\alpha_k \sigma_k}{4}\right) L_i,$$

Table 1
Geometrical parameters and thermophysical properties of the gas phase and of the particle phase k

Gas phase	Particle phase
$\lambda_g = 0.0035$ W m^{-2} K^{-1}	$\rho_k = 510$ kg m^{-3}
$\rho_g = 0.8$ kg m^{-3}	$c_{pk} = 1380$ J kg^{-1} K^{-1}
$c_{pg} = 1.02$ J kg^{-1} K^{-1}	$\varepsilon_k = 1$
$\beta_g = 0.5$ m^{-1}	$d_k = 0.002$ m $\Rightarrow \sigma_k = 3000$ m^{-1}
$\omega_g = 1$	$\alpha_k = 0.001$

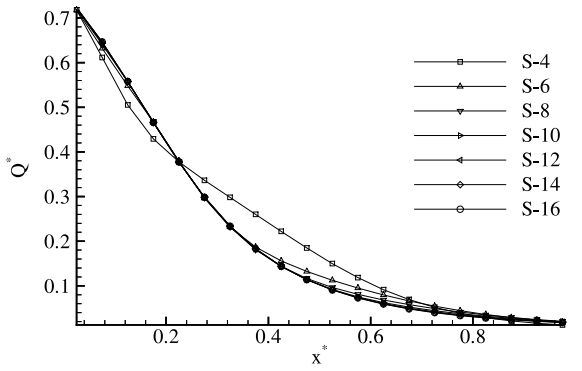

Fig. 7. SN approximation effects on the dimensionless centerline net radiative flux in the x-direction.

$$\tau_{k_i} = \frac{\alpha_k \sigma_k}{4} L_i,$$

and the mean free path length for radiation through the particle phase is

$$\delta_k = \frac{4}{\alpha_k \sigma_k} = 1.33 \text{ m}.$$

4.2.2. Quadrature effects

Fig. 7 shows the dimensionless centerline net flux versus $x^* = x/L_x$ predicted using $S-4$ to $S-16$ approximations. The ray effects appear distinctly in the shape of curves. The lack of accuracy of quadratures $S-4$ and $S-6$ is clear. If $S-16$ is taken as a reference solution the average deviations of the solutions provided by the other quadratures are given in Table 2.

The best compromise between accuracy and an acceptable computing time is the quadrature $S-12$. In so far as a single qualitative study is undertaken, the approximation $S-12$ will subsequently be used.

4.2.3. Effects of the particle-phase specific surface

In this section, the influence of the specific surface of the particle phase is considered when both phases are considered to be absorbing–emitting but non-scattering. It depends only on two parameters, namely the particle-phase number density n_k and the particle surface s_{pk}:

Table 2
$S-8$ to $S-14$ deviations vs. $S-16$ in the calculation of the dimensionless centerline net radiative flux in the x-direction

Quadrature	Mean deviation (%)	Maximum deviation (%)
$S-14$	1	3.7
$S-12$	4.5	8.6
$S-10$	6.3	14.3
$S-8$	8.8	21.8

$$A_k = \alpha_k \sigma_k = n_k v_{pk} \sigma_k = n_k s_{pk}. \tag{49}$$

An increase of one of this two parameters causes the specific surface to increase. Three cases are considered:

$$A_k = 0.3 \text{ m}^{-1} \Rightarrow \tau_{kx} = 0.15 \Rightarrow \delta_k = 13.33 \text{ m}, \tag{50}$$

$$A_k = 3 \text{ m}^{-1} \Rightarrow \tau_{kx} = 1.5 \Rightarrow \delta_k = 1.33 \text{ m}, \tag{51}$$

$$A_k = 30 \text{ m}^{-1} \Rightarrow \tau_{kx} = 15 \Rightarrow \delta_k = 0.133 \text{ m}. \tag{52}$$

This leads to a decrease of the mean free path length for radiation in the particle phase δ_k. It follows that the radiative intensity is attenuated over a shorter distance as shown on the incident radiative flux along the vertical midline at the east cold wall given in Fig. 8(a). On the other hand, the opposite phenomena occur on the hot wall Fig. 8(b).

When the optical thickness is increased, the flux in direction x^+ is weaker (Fig. 8(c)) while the flux in direction x^- increases as a result of greater absorption in the particle phase and thus a higher re-emission, particularly near the hot wall (Fig. 8(d)). The competition between the transmission and emission phenomena explains the incident radiative field's behavior given in Fig. 8(e).

4.2.4. Gas scattering effects

The effects of isotropic and anisotropic gas scattering are examined and the scattering albedo is taken as $\omega_g = 0.7$. In the anisotropic case, the gas diffusion is assumed to come from medium-size particles ($0.3 < \chi < 5$). In this case, gas scatters anisotropically using Legendre phase function expansion [4].

When expressing the phase function as a finite series approximation of Legendre polynomials, a forward ($F1$) or a backward ($B2$) scattering may be described. The scattering phase functions for $F1$ and $B2$ proposed by Kim et al. [21] are used.

$$\Phi_g^{\Omega\Omega'} = 1 + \sum_{m=1}^{\infty} a_m P_m(\cos\psi). \tag{53}$$

The values of polynomial coefficient a_m corresponding to $F1$ and $B2$ used are shown in Table 3. The different scattering phase functions are plotted in Fig. 3.

Fig. 9(a) and (b) show the dimensionless centerline radiative flux in the x^+ and x^- directions. The results obtained by functions $F1$ and $B2$ are in agreement with their respective forward and backward scattering characters. This is confirmed by Fig. 9(c) and (d) which represent the incident fluxes at the center of the hot and cold walls, respectively, versus $y^* = y/L_y$. The results obtained without and with isotropic scattering are virtually identical. The negligible influence of the phase function on the gas temperature distribution is illustrated in Fig. 9(e). Deviations between non-scattering

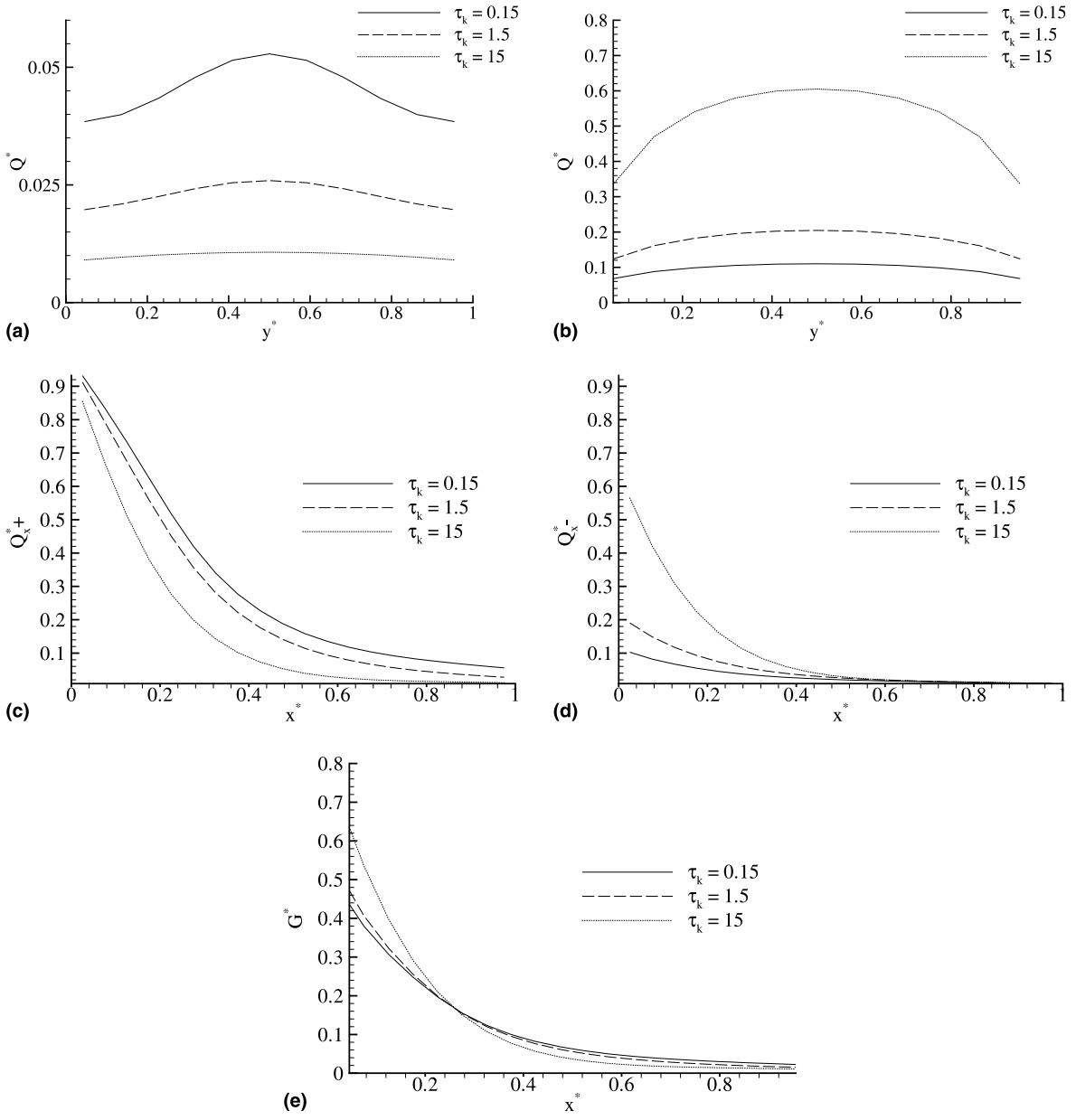

Fig. 8. Effects of particle-phase optical thickness on the dimensionless incident radiative flux (a) at the cold wall, (b) at the hot wall, on the dimensionless radiative flux (c) in the positive x-direction, (d) in the negative x-direction, and (e) on the dimensionless average incident radiation.

and scattering conditions are low (6% for $F1$ and 2% for $B2$) despite the high albedo. As pointed out by Park et al. [8], this behavior can be explained by the scattering-induced redistribution of the radiative intensity and the isotropic emission.

The effects of scattering are studied when a high-temperature source is placed in the enclosure. A uniform volumetric heat source of 5 kW m^{-3} is considered. All the enclosure walls are assumed to be black and cold (300 K). In this case, the medium evacuates the heat towards the wall by emitting strongly and the conduction exchanges between the particles and the gas are no longer negligible. As shown in Fig. 10 predictions of the centerline temperature distribution for either isotropic,

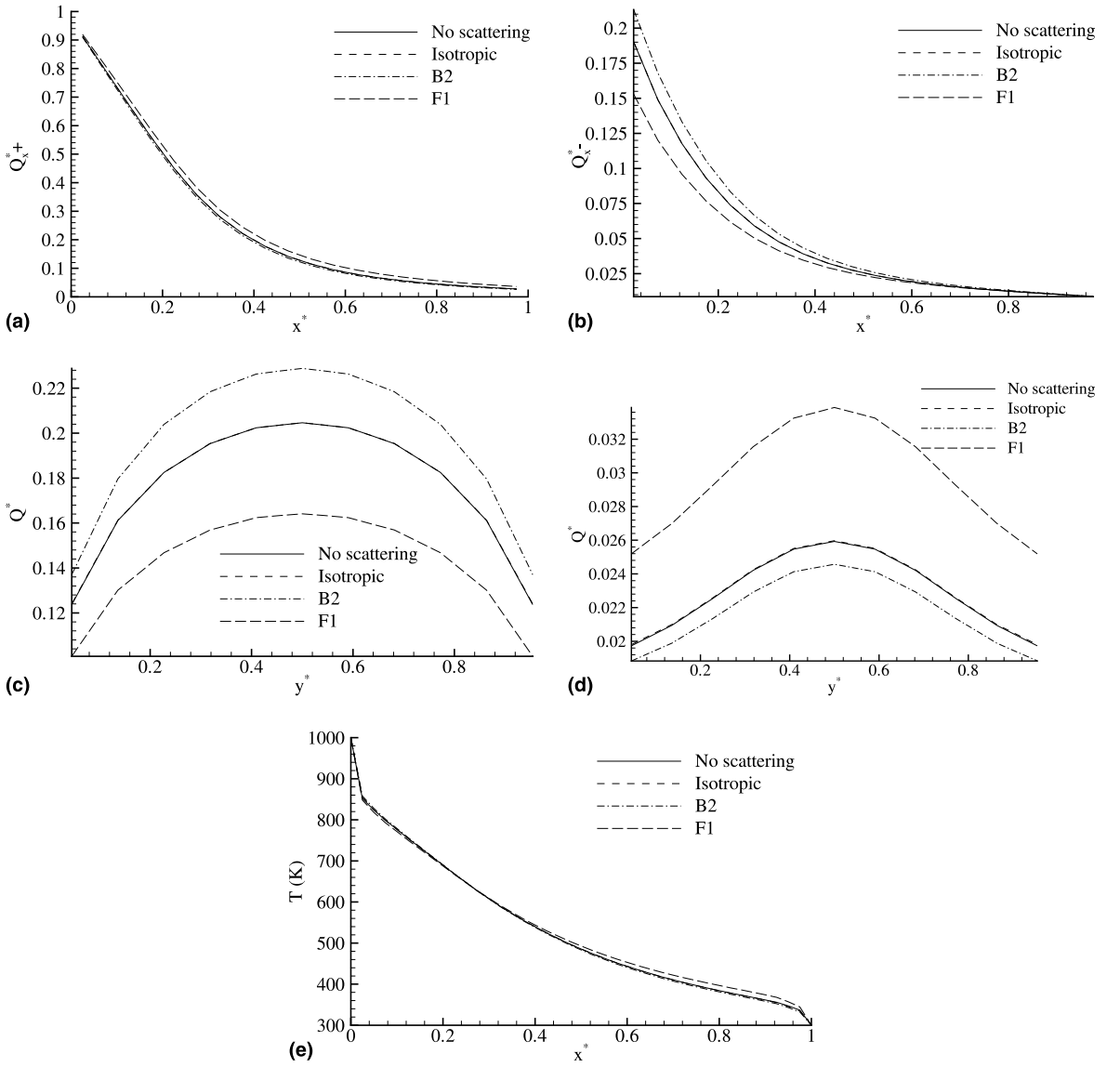

Fig. 9. Effects of gas scattering phase functions on the dimensionless radiative flux (a) in the positive x-direction and (b) negative x-direction, on the dimensionless incident radiative flux (c) at the hot wall, (d) at the cold wall, and (e) on the gas temperature distribution – differentially heated enclosure.

$F1$ or $B2$ scattering conditions are qualitatively the same. As observed by Kim and Lee [21] for a gaseous medium, scattering anisotropy is ineffective when symmetrical conditions are imposed. Unlike the previous case, the results obtained with and without isotropic scattering differ noticeably. The baseline case of no scattering results in a higher gas absorption which leads to a stronger emission. The energy released by the volumetric source is evacuated more easily and causes a smaller temperature increase.

4.2.5. Particle scattering effects

The particles here will be considered as diffuse gray and the diffraction is neglected for the reasons given before. The diffuse reflection for large spherical particles is modeled by the phase function given by Eq. (48). The effects of the particle reflectivity $(1-\varepsilon_k)$ on the dimensionless incident flux profiles at the hot and cold walls are illustrated in Fig. 11(a) and (b). The results obtained for emissivities of 0.9 and 1 are close with average deviations of 2.1% and 1.3% for the hot

Table 3
Polynomial coefficients of the Legendre expansion for the $F1$ and $B2$ scattering phase functions

$F1$	$B2$
$a_0 = 1$	$a_0 = 1$
$a_1 = 2.53602$	$a_1 = -1.2$
$a_2 = 3.56549$	$a_2 = 0.5$
$a_3 = 3.97976$	
$a_4 = 4.00292$	
$a_5 = 3.66401$	
$a_6 = 3.01601$	
$a_7 = 2.23304$	
$a_8 = 1.30251$	
$a_9 = 0.53463$	
$a_{10} = 0.20136$	
$a_{11} = 0.0548$	
$a_{12} = 0.01099$	

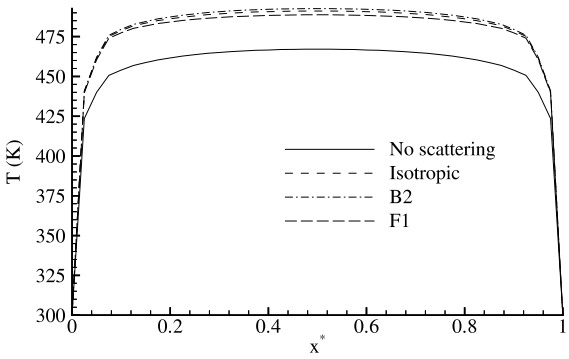

Fig. 10. Effects of gas scattering phase functions on the gas temperature distribution – enclosure with a high-temperature source.

and cold walls, respectively. In addition, the centerline temperature distribution is fairly sensitive to this parameter since the maximum deviation is less than 3% (Fig. 11(c)). These findings reinforce the mathematical validity of the approximation that the particles, whose emissivity is greater than 0.7, can be considered to be black.

For the heat source case, this sensitivity becomes more pronounced (Fig. 12). Maximum deviations vs. the blackbody approximation are given in Table 4.

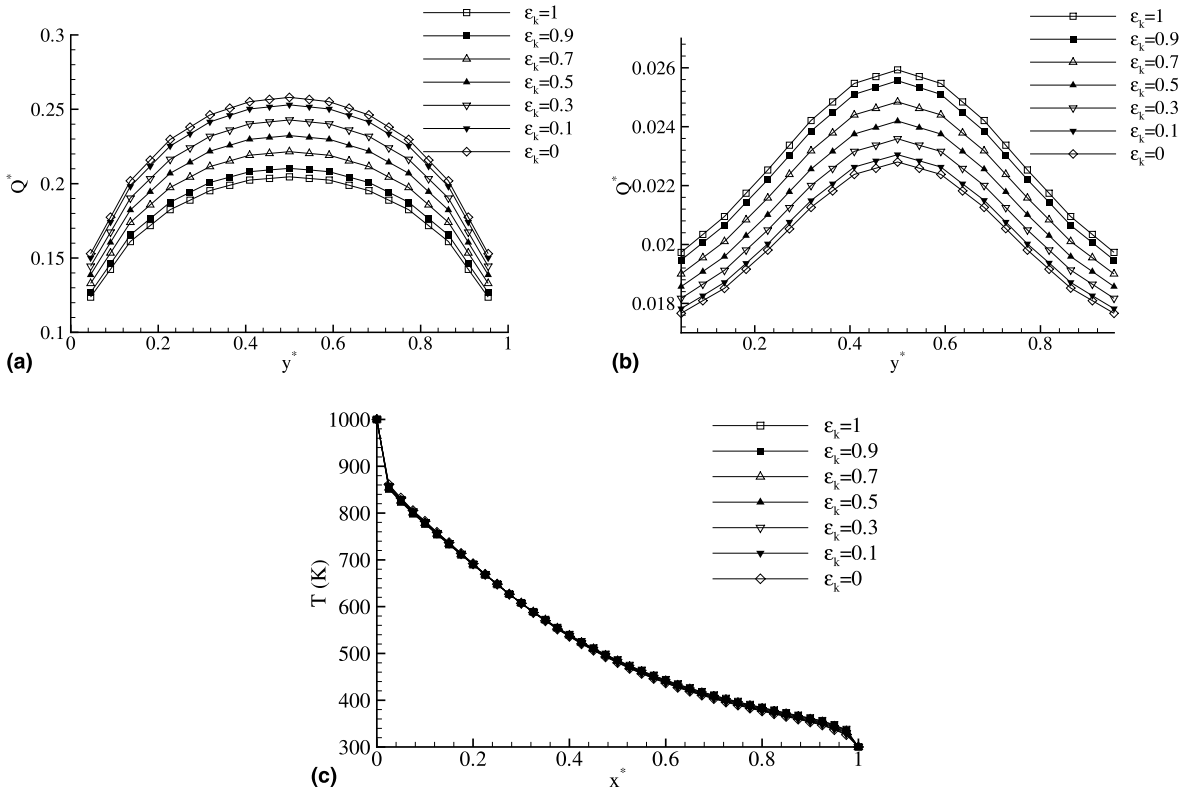

Fig. 11. Particles emissivity effects on the incident radiative flux (a) at the hot wall and (b) at the cold wall, and (c) on the gas temperature distribution – differentially heated enclosure.

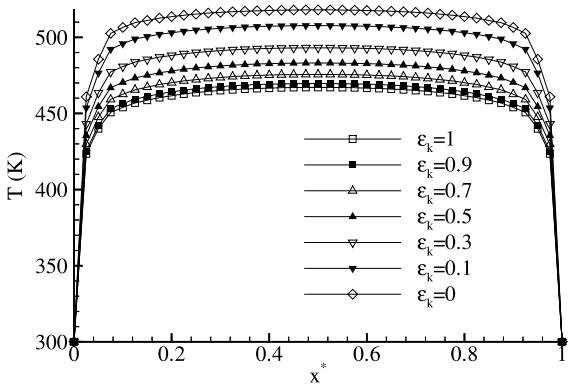

Fig. 12. Particles emissivity effects on the gas temperature distribution – enclosure with a high-temperature source.

Table 4
Maximum deviation in gas temperature distribution for different particle emissivities vs. that obtained with black particles – enclosure with a high-temperature source

Particle emissivity	Deviation vs. blackbody (%)
0.9	<1
0.7	1.8
0.5	3.4
0.3	5.6
0.1	8.6
0	10.9

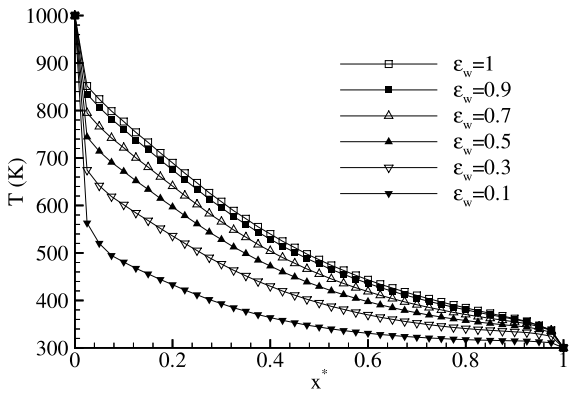

Fig. 13. Wall emissivity effects on the gas temperature distribution.

4.2.6. Effects of the wall emissivity

The influence of the emissivity of the walls $x = 0$ and $x = L_x$ on the temperature profile is considered and plotted in Fig. 13. As expected, the influence of the wall emissivity is great. It is clear that a reduction in the emissivity involves a reduction in the temperature field. It is found that a change in wall emissivity from 0.3 to 0.7 may cause a 21% temperature difference.

5. Conclusions

In the present work, radiative transfers in multiphase media composed of a gas phase and several particle phases are modeled using a formal averaging procedure. A MRTE which considers absorption, emission and scattering for each phase is derived. Large, spherical, opaque particles are considered. The MRTE is solved by the discrete ordinate method and good quantitative agreement is obtained with experiments and Monte-Carlo simulations. The multiphase energy balance equation for both particle and gas phases are obtained by using the same averaging method and then coupled to the MRTE to describe combined radiative and conductive heat transfers in multiphase media. Results are presented for a differentially heated three-dimensional rectangular enclosure and for a three-dimensional enclosure containing a high-temperature heat source. The following conclusions can be drawn:

- The multiphase model solutions follow correct trends.
- The parameter which characterizes the action of the particle phases is the specific exchange surface. An increase in this parameter reduces the transparency of the medium and the radiative energy is trapped near the hot wall.
- The gas scattering was modeled by phase functions $F1$ and $B2$. The model with isotropic scattering really differs (5.5%) from the non-scattering model in the presence of a volumetric source only. Moreover the results obtained with the forward scattering $F1$ and backward $B2$ are close (<7%) to those obtained with the isotropic scattering model.
- To simulate the particle-phase scattering the diffuse reflection model was used. It would seem that for emissivity of 0.9 (even 0.7), a real particle may be considered at a first approximation to be black body.

A logical follow up to this study will be to envisage non-opaque particles and thus to have a general model.

Appendix A. Mathematical theorems used in the formal averaging method

The use of the weighting function leads to a multiphase formulation of the Leibnitz rule and Gauss theorem.

For the gas phase

$$\int_{V_{g\infty}} g\frac{\partial a_g}{\partial y_i}\,\mathrm{d}V = \frac{\partial}{\partial x_i}(\alpha_g\langle a_g\rangle) + \sum_{k=1}^{N}\sum_{p=1}^{P_k}\int_{s_{pk}} g a_g n_i\,\mathrm{d}s,$$

$$\int_{V_{g\infty}} g\frac{\partial a_g}{\partial t}\,dV = \frac{\partial}{\partial t}(\alpha_g\langle a_g\rangle) - \sum_{k=1}^{N}\sum_{p=1}^{P_k}\int_{s_{pk}} g a_g v_i n_i\,ds,$$

in which v_i is the local velocity component at s_{pk}. For the particle phase k,

$$\sum_{p=1}^{P_k}\int_{V_{k\infty}} g\frac{\partial a_k}{\partial y_i}\,dV = \frac{\partial}{\partial x_i}(\alpha_k\langle a_k\rangle) + \sum_{p=1}^{P_k}\int_{s_{pk}} g a_k n_i\,ds,$$

$$\sum_{p=1}^{P_k}\int_{V_{k\infty}} g\frac{\partial a_k}{\partial t}\,dV = \frac{\partial}{\partial t}(\alpha_k\langle a_k\rangle) + \sum_{p=1}^{P_k}\int_{s_{pk}} g a_k v_i n_i\,ds.$$

In the present study $v_i = 0$. Moreover, in order to express particle/gas interaction terms and assuming that the weighting function varies little at the surface of a single particle, we can write [12] for any property A:

$$\sum_{p=1}^{P_k}\int_{s_{pk}} g(r)A(\mathbf{y};t)\,ds \approx \sum_{p=1}^{P_k} g_{pk}\int_{s_{pk}} A(\mathbf{y};t)\,ds. \tag{A.1}$$

In addition, if A is considered as constant at the particle surface, we can write

$$\sum_{p=1}^{P_k}\int_{s_{pk}} g(r)A(\mathbf{y};t)\,ds \approx \sum_{p=1}^{P_k} g_{pk}s_{pk}A_p \tag{A.2}$$

$$= \sum_{p=1}^{P_k} g_{pk}v_{pk}(\sigma_k A_p) \approx \alpha_k\langle\sigma_k A\rangle. \tag{A.3}$$

The conjugate action of the two topological parameters is so pointed out.

References

[1] B.J. Mason, The Physics of Clouds, Clarendon Press, Oxford, 1971.

[2] E.F. Harrison, P. Minnis, B.R. Barkstrom, V. Ramanathan, R.D. Cess, G.G. Gibson, Seasonal variation of cloud radiative forcing derived from the earth radiation budget experiment, J. Geophys. Res. 95 (1990) 18687.

[3] K.F. Evans, The spherical harmonics discrete ordinate method for three-dimensional atmospheric radiative transfer, J. Atmos. Sci. 55 (1998) 429–446.

[4] M.F. Modest, Radiative Heat Transfer, McGraw-Hill, New York, 1993.

[5] Y.S. Yang, J.R. Howell, D.E. Klein, Radiative heat transfer through a randomly packed beds of spheres by the Monte Carlo method, J. Heat Transfer 105 (1983) 325–332.

[6] G.D. Mazza, C.A. Berto, G.F. Barreto, Evaluation of radiative heat transfer properties in dense particulate media, Powder Technol. 67 (1991) 137–144.

[7] C.L. Tien, B.L. Drolen, Thermal radiation in particulate media with dependent and independent scattering, Ann. Rev. Numer. Fluid Mech. Heat Transfer 1 (1987) 1–32.

[8] J.H. Park, S.W. Baek, S.J. Kwon, Analysis of a gas–particle direct-contact heat exchanger with two-phase radiation effect, Numer. Heat Transfer, Part A 33 (1998) 701–721.

[9] K.M. Kim, H.J. Lee, S.W. Baek, Analysis of two-phase radiation in thermally developing Poiseille flow, Numer. Heat Transfer, Part A 36 (1999) 489–510.

[10] B.P. Singh, M. Kaviany, Independent theory versus direct simulation of radiation heat transfer in packed beds, Int. J. Heat Mass Transfer 34 (1991) 2869–2882.

[11] B.P. Singh, M. Kaviany, Modeling radiative heat transfer in packed beds, Int. J. Heat Mass Transfer 35 (1992) 1397–1405.

[12] T.B. Anderson, R. Jackson, A fluid mechanical description of fluidized beds, IECh Fundam. 6 (1967) 527–539.

[13] P.S. Gough, F.J. Zwarts, Modeling heterogeneous two-phase reacting flow, AIAA J. 17 (1979) 17–25.

[14] G.D. Mazza, S.P. Bressa, G.F. Barreto, On validity of the addition of independent contributions for evaluating heat transfer rates in gas fluidized beds, Powder Technol. 90 (1997) 1–11.

[15] J.M. Delhaye, Local instantaneous equations, instantaneous space-averaged equations, two-phase and heat transfer, in: Proceedings of NATO Advanced Study Institute, Istambul, vol. 1, 1976.

[16] S. Chandrasekhar, Radiative Transfer, Dover, New York, 1960.

[17] K.D. Lathrop, F.W. Brinkley, TWOTRAN-2: an interfaced, exportable version of the TWOTRAN code for two-dimensionnal transport, Los Alamos Scientific Laboratory, Report no. LA-4848-MS, 1973.

[18] K.D. Lathrop, Spacial differencing of the transport equation: positivity vs. accuracy, J. Comput. Phys. 4 (1969) 475–498.

[19] S.V. Patankar, Numerical Heat Transfer and Fluid Flow, Series in Computational Methods in Mechanics and Thermal Science, Hemisphere, New York, 1980.

[20] J.C. Chen, S.W. Churchill, Radiant heat transfer in packed beds, AIChE J. 8 (1963) 35–41.

[21] T.K. Kim, H. Lee, Effect of anisotropic scattering on radiative heat transfer in two-dimensional rectangular enclosures, Int. J. Heat Mass Transfer 31 (1988) 1711–1721.